Zeolite (MFI) Crystal Morphology Control Using Organic Structure-Directing Agents

Griselda Bonilla,[‡] Isabel Díaz,[†,‡,¶] Michael Tsapatsis,*[,†] Hae-Kwon Jeong,[†] Yongjae Lee,[§] and Dionisios G. Vlachos[||]

Department of Chemical Engineering and Materials Science, University of Minnesota, Minneapolis, Minnesota 55455, Department of Chemical Engineering, University of Massachusetts, Amherst, Massachusetts 01003, Physics Department, Brookhaven National Laboratory, Upton, New York 1197, Department of Chemical Engineering, University of Delaware, Newark, Delaware 19716

Received July 14, 2004. Revised Manuscript Received September 20, 2004

The effect of structure-directing agents (SDAs) on zeolite particle morphology and crystal structure was studied. Dimers and trimers of tetrapropylammonium hydroxide—the SDA of siliceous ZSM-5 (silicalite-1, structure type MFI)—lead to direct growth of the same framework but with drastically different crystal morphologies. Control over relative crystal growth rates along the three main crystallographic axes is demonstrated by obtaining crystals with their longest dimension along any of these axes. Unit cell dimensions and crystal structure were determined by refinement based on powder X-ray diffraction data and electron microscopy, respectively. The importance of the new morphologies in thin film molecular sieve technology along with possible crystal growth mechanisms is discussed.

Introduction

Zeolites are crystalline microporous aluminosilicates with precisely defined cages and channels at the nanometer scale. The ability to control the particle size and shape of a given zeolite structure is desirable not only for applications in catalysis and adsorption,[1,2] but also for a variety of uses of these zeolite particles as seeds for the growth of zeolite membranes,[3−6] for synthesis of polymer-zeolite composites,[7,8] or as building blocks for the construction of hierarchical porous crystalline structures.[9] Fine-tuning of zeolite crystal size and shape is usually accomplished by systematic variation of the composition of the precursor mixture (including the use of additives such as salts) and of synthesis parameters such as temperature and stirring rate during hydrothermal synthesis. Synthesis in microstructured media like polymer hydrogels[10] and reverse micelles[11,12] has also been successfully employed to further enhance the ability to control zeolite particle size and possibly shape. Here, we focus on the use of structure-directing agents (SDAs), not to guide the formation of a certain zeolite crystal structure,[13−15] but to systematically manipulate the zeolite crystal shape. Although elements of this idea can be encountered throughout the zeolite literature, we found no quantitative experimental study on the effect of SDAs on crystal shape for a given zeolite structure and composition. More specifically, we report here the effect of SDAs on the synthesis of siliceous ZSM-5 (structure type MFI), an important catalyst and promising membrane material.

The most commonly used SDA for siliceous ZSM-5 or silicalite-1 is the tetrapropylammonium cation (TPA). The characteristic crystal shape of TPA-silicalite-1 is a hexagonal prismatic shape, more commonly referred to as a coffin shape with the order of crystal dimensions $L_c \geq L_a > L_b$ (where L_i indicates crystal size along i-axis) as shown in Figure 1. This shape is observed for various synthesis conditions in the presence of TPA. However, earlier studies indicate the potential for a drastic change in the MFI crystal morphology by using a certain class of quaternary ammonium SDAs.[16] De Vos Burchart and co-workers reported on the synthesis of silicalite-1

* Corresponding author. E-mail: tsapatsi@cems.umn.edu. Tel: +1- 612-626-0920. Fax: +1- 612-626-7246.
† University of Minnesota.
‡ University of Massachusetts.
§ Brookhaven National Laboratory.
|| University of Delaware.
¶ Currently at the Instituto de Catálisis y Petroleoquímica, CSIC, Campus Cantoblanco, 28049-Madrid, Spain.

(1) Yates, M. Z.; Ott, K. C.; Birbaum, E. R.; McCleskey, T. M. *Angew. Chem. Int. Ed.* **2002**, *41*(3), 476−478.
(2) Bedard, R. L. *AIChE J.* **1999**, *45*(12), 2474−2476.
(3) Mintova, S.; Valtchev, V.; Engstrom, V.; Schoeman, B. J.; Sterte, J. *Microporous Mater.* **1997**, *11*(3−4), 149−160.
(4) Ha, K.; Lee, Y. J.; Lee, H. J.; Yoon, K. B. *Adv. Mater.* **2000**, *12*(15), 1114−1117.
(5) Lai, Z. P.; Bonilla, G.; Diaz, I.; Nery, J. G.; Sujaoti, K.; Amat, M. A.; Kokkoli, E.; Terasaki, O.; Thompson, R. W.; Tsapatsis, M.; Vlachos, D. G. *Science* **2003**, *300*(5618), 456−460.
(6) Yuan, W. H.; Lin, Y. S.; Yang, W. S. *J. Am. Chem. Soc.* **2004**, *126*(15), 4776−4777.
(7) Koros, W. J.; Mahajan, R. *J. Membr. Sci.* **2000**, *175*(2), 181−196.
(8) Wang, H. T.; Holmberg, B. A.; Yan, Y. S. *J. Mater. Chem.* **2002**, *12*(12), 3640−3643.
(9) Huang, L. M.; Wang, Z. B.; Sun, J. Y.; Miao, L.; Li, Q. Z.; Yan, Y. S.; Zhao, D. Y. *J. Am. Chem. Soc.* **2000**, *122*(14), 3530−3531.
(10) Wang, H. T.; Holmberg, B. A.; Yan, Y. S. *J. Am. Chem. Soc.* **2003**, *125*(33), 9928−9929.
(11) Dutta, P. K.; Robins, D. *Langmuir* **1991**, *7*, 1048−1050.
(12) Singh, R.; Dutta, P. K. *Langmuir* **2000**, *16*(9), 4148−4153.
(13) Lewis, D. W.; Willock, D. J.; Catlow, C. R. A.; Thomas, J. M.; Hutchings, G. J. *Nature* **1996**, *382*(6592), 604−606.
(14) Lok, B. M.; Cannan, T. R.; Messina, C. A. *Zeolites* **1983**, *3*, 282−291.
(15) Davis, M. E.; Lobo, R. F. *Chem. Mater.* **1992**, *4*, 756−768.

10.1021/cm048854w CCC: $27.50
Published on Web 11/26/2004

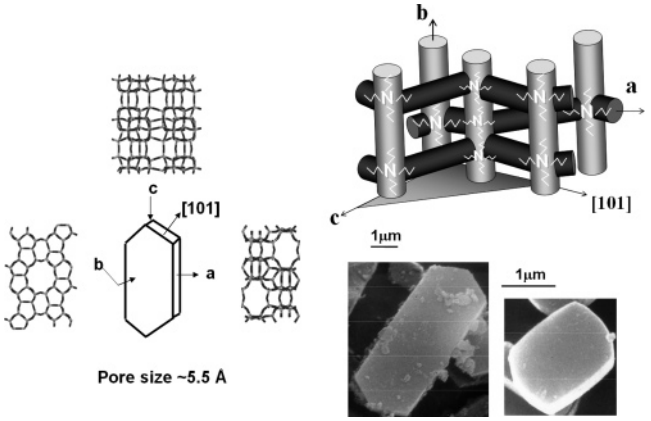

Figure 1. Schematic of the pore structure of TPA-MFI with the TPA located at channel intersections (top right). Typical SEM images of coffin-shaped crystals are shown at the bottom right of the figure. A schematic identifying the crystal faces and directions along with the corresponding framework projections is shown on the left part of the Figure.

crystals with $L_b > L_a$ using dimer C6 TPA cations ($((C_3H_7)_3N^+(CH_2)_6\ N^+(C_3H_7)_3$) as the SDA.[17] They attributed this change to a better fit of the dimer in the straight (along *b*-axis) versus the sinusoidal (along *a*-axis) channels of silicalite-1. In this communication, we investigate the role of this class of SDAs (i.e., diquaternary and triquaternary cations) on crystal morphology. Specifically, we report on the use of diquaternary ammonium cations, $(C_3H_7)_3N^+(CH_2)_n\ N^+(C_3H_7)_3$, where n varies between 5 and 7 (noted as dC5, dC6, and dC7, respectively), as well as the trimer C6 TPA cations (noted as tC6) as SDAs for the synthesis of silicalite-1 with the objective of altering the crystal shape.

Experimental Section

SDA Synthesis. TC6 was prepared by exhaustive alkylation of bis(hexamethylene)triamine with 1-iodopropane. Approximately 450 mL of the solvent 2-butanone, 72.6 g of anhydrous potassium carbonate (HI and water scavenger), and 27.87 g of the triamine were added to a dry three-necked 1-L flask equipped with a mechanical stirrer, a 60-mL addition funnel, and a reflux condenser. The reaction flask was then flushed with purified argon gas and vented through a bubbler. Iodopropane, 101 mL, was quickly transferred to the addition funnel. The reaction mixture was slowly heated to reflux (approximately 85 °C) under argon as the iodopropane was added dropwise to the stirring mixture. The reaction was kept in the dark to avoid iodide oxidation. After approximately 10 h, the warm, bright yellow reaction mixture was filtered to remove the potassium salts. The 2-butanone was removed by rotary evaporation resulting in an off-white semisolid. The first step of the purification protocol consisted of the addition of cold 2-butanone to the crude product followed by stirring for 1 h. An equal amount of ethyl acetate was slowly added to the stirring mixture. After standing for over 10 h, the solid product was recovered from the solution by filtration. Then, traces of KI were separated from the product by dissolving the product in a minimum of 200 proof ethanol. The KI was filtered and the solvent was then removed by rotary evaporation. The product was then recrystallized a second time following the first step of the purification protocol. The entire purification protocol was subsequently repeated a second time (40 g, 33% yield). The purity of the compound was verified using elemental analysis (C,H,N) and ^{13}C NMR δ (normalized intensity): 10.3(2), 15.4(2), 21.6(1), 25.6(1), 58.7(1), 60.3(2). DC6 was prepared by exhaustive alkylation of 1,6-diaminohexane with 1-iodopropane (108 mL). The synthesis protocol is similar to that of the tC6 using a mixture of approximately 450 mL of the solvent 2-butanone, 82.35 g of anhydrous potassium carbonate, and 21.50 g of the diamine. The tC6 purification protocol was followed and the ^{13}C NMR δ (normalized intensity) is 9.9(3), 14.9(3), 21.1(1), 25.1(1), 58.2(1), 59.8(3). DC7 was prepared by exhaustive alkylation of 1,7-diaminoheptane with 1-iodopropane (108 mL). The synthesis procedure is similar to that of the tC6 using a mixture of approximately 450 mL of the solvent 2-butanone, 82.35 g of anhydrous potassium carbonate, and 24.09 g of the diamine. The purification steps are similar to those described above, with the exception that the solvents used for the recrystallization are acetone and ethyl ether. The ^{13}C NMR δ (normalized intensity) is 10.9(6), 15.9(6), 22.0(2), 26.3(2), 28.5(1), 59.4(2), 61.0(6). DC5 was prepared by exhaustive alkylation of 1,5-diaminopentane with 1-iodopropane (108 mL). The synthesis procedure is similar to the previous ones using a mixture of approximately 450 mL of the solvent 2-butanone, 82.35 g of anhydrous potassium carbonate, and 18.90 g of the diamine. The purification procedure followed is the same as described for tC6. The ^{13}C NMR δ (normalized intensity) is 11.0(6), 16.0(6), 22.1(1), 23.8(2), 59.1(2), 61.1(6).

Zeolite Synthesis. The zeolite synthesis mixture was prepared by first dissolving a specified amount of the SDA in a 0.85 M solution of KOH (85%, EM Science) and distilled water. Thereafter, the silica source, tetraethyl orthosilicate (98%, Aldrich), was added. The final molar composition of the synthesis mixture was $40SiO_2$:$(15/x)SDA^{+x}xI^-$:25KOH:9500H_2O:160EtOH, where x corresponds to the number of nitrogen atoms in the particular SDA. N^+/Si was kept constant at 0.375, such that the corresponding value of x is 0.375, 0.1875, and 0.125 for TPA, the dimers of TPA, and the trimer TPA, respectively. For seeded synthesis experiments, 400 μL of a 20 g/L suspension of colloidal (calcined) silicalite-1 seeds was added to the synthesis mixture using disposable 100-μL micropipets (Drummond Scientific). Parallel nonseeded syntheses were also performed to study the crystal morphology as well as the nucleation behavior.

The reaction mixtures were stirred at room temperature for 5 h, after which a clear solution (by visual inspection) was obtained. The synthesis mixture was then filtered into Teflon-lined 45-mL stainless steel autoclaves and heated to synthesis temperatures of 130 °C or 175 °C under autogenous pressure and rotation. After a fixed reaction time, the autoclaves were removed and quenched cool in a water bath. The solid products were recovered by centrifugation at 11 000 rpm for 15 min followed by decantation, after which they were redispersed in distilled water. This washing treatment was repeated five times. The crystals were then dried for 5 h at 90 °C. Calcination of the crystals (for removal of the SDA) was performed by heating from room temperature at a rate of 0.5 °C/min to 480 °C for 10 h, followed by cooling back to room temperature at a rate of 0.5 °C/min.

Characterization. Several different experimental techniques were used to study the structure and morphology of the silicalite-1 crystals.

Crystallinity, phase purity, and identification of the solids were determined by powder X-ray diffraction (XRD) patterns collected on a Philips X-Pert system using CuKα radiation in a $\theta/2\theta$ geometry. To get refinable quality data, synchrotron powder X-ray diffraction patterns were collected at beamline ×7A at the National Synchrotron Light Source (NSLS) with monochromatic X-ray radiation ($\lambda \sim 0.9$ Å). Unit cell parameters were determined by whole pattern fitting using the LeBail method with EXPGUI/GSAS package.[18,19] The diffraction peaks were modeled using the pseudo-Voigt profile function.

The amount of organic occluded in the product was determined using a thermogravimetric analyzer (TA Instruments,

(16) Jansen, J. C. In *Introduction to Zeolite Science and Practice*; van Bekkum, H., Flanigen, E. M., Jansen, J. C., Eds.; Elsevier Science: Amsterdam, 1991; Vol. 58, pp 125−127.

(17) de Vos Burchart, E.; Jansen, J. C.; van de Graaf, B.; van Bekkum, H. *Zeolites* **1993**, *13*, 216−221.

Table 1. Silicalite-1 Crystal Sizes (in μm) Reported for Both Seeded and Nonseeded Syntheses with a Molar Composition of $40SiO_2$:$(15/x)SDA^x$+xI^-: 25KOH:9500H_2O:160EtOH[a]

	(μm)	TPA	dC7	dC6	tC6	dC5[c]
seeded	L_c	0.4 ± 0.0	0.4 ± 0.0	[b]	0.4 ± 0.0	0.1 ± 0.0
	L_a	0.3 ± 0.0	0.3 ± 0.0		0.2 ± 0.0	0.1 ± 0.0
	L_b	0.2 ± 0.0	0.1 ± 0.0		0.4 ± 0.0	0.2 ± 0.0
nonseeded	L_c	14.1 ± 0.2	1.5 ± 0.0	10.9 ± 0.2	2.3 ± 0.0	3−8
	L_a	10.5 ± 0.2	1.2 ± 0.0	2.9 ± 0.1	0.5 ± 0.0	10−20
	L_b	5.8 ± 0.1	0.4 ± 0.0	3.1 ± 0.1	1.7 ± 0.0	1−2

[a] Where x corresponds to the number of nitrogens in the SDA. Syntheses were performed at 175 °C for 24 h. The seeded crystal sizes reported here are before subtracting the size of the original colloidal seed crystal that has a size of approximately 0.11 μm. [b] Seeded growth experiments using dC6 as the SDA yield leaf-shaped crystals that are aggregated with multiple intergrowths (see Supp. Info. S3) such that accurate quantitative size measurements along the different crystallographic axes are not possible. [c] Seeded synthesis at 175 °C yields plates and cylinders. Nonseeded synthesis at 175 °C yields plates. The reported dimensions for seeded synthesis are only for cylinders. The dimensions given for nonseeded synthesis are for plates.

Inc. TGA 2950), in which 5−12-mg samples were heated in air at rates of 10 °C/min.

^{13}C NMR spectroscopy was used to determine if the template was occluded intact within the zeolite. The solid-state spectra were collected on a Bruker DSX300 instrument with magic-angle spinning (MAS) 7-mm zirconia rotors at 4−5 kHz. Cross polarization used a H 90° pulse length of 5 μs, a recycle delay of 6.6s, and a cross-polarization period of 2 ms.^{13}C NMR spectral chemical shifts were externally referenced to sodium trimethylsily-proprionate-2,2,3,3.

Crystal morphology and size were determined using scanning electron microscopy (SEM). The samples were dispersed onto carbon tape and coated with a gold/palladium alloy using a Polaron E5100 Sputter Coater System. The zeolite crystals were then observed on a JEOL JSM-5400 microscope operating in SEM mode at 15 kV. An average of ~20 crystals was used to measure the dimensions of the crystals along the three crystallographic axes.

Transmission electron microscopy (TEM) coupled with selected area electron diffraction (SAED) was used to index the crystal faces. Three microscopes were used for this work: JEOL 4000, 400 kV; JEOL ARM 1250, 1250 kV; and a Philips CM30, 300 kV. For TEM analysis, the samples were first dispersed in acetone and then placed on a holey carbon microgrid.

Results and Discussion

Synthesis with TPA, dC7, dC6, and tC6. Scanning electron microscopy (SEM) was used to observe the shape of silicalite-1 crystals. Product crystals obtained from nonseeded syntheses at 175 °C in the presence of TPA, dC7, dC6, and tC6 are shown in Figure 2a−d, respectively. XRD analysis confirms that the as-synthesized zeolite crystals presented here are structure type MFI (Figure S1, Supp. Info.). In addition, at these synthesis conditions, the presence of the same peaks in the ^{13}C NMR spectra of the SDA in solution compared to the SDA-zeolite confirms that the SDA is occluded intact inside the zeolite lattice (Figure S2, Supp. Info.). Seeded syntheses yield crystals with the same characteristic shape as the corresponding nonseeded syntheses with the exception that the crystals are generally smaller in size (see Table 1), and in some cases crystal aggregation and intergrowth are more pronounced (i.e., dC6 synthesis shown in Supp. Info S3).

Transmission electron microscopy (TEM) images coupled with selected area electron diffraction (SAED) patterns were used to identify the corresponding crystal faces. The smaller zeolite crystals obtained from the seeded synthesis using dC7, dC6, and tC6 were calcined prior to the TEM/SAED analysis and are shown in Figure 3a−e, respectively. By tilting the crystals, it is possible to align the b and a directions, that is, straight and sinusoidal channels, parallel to the electron beam. Figure 3b and d shows that the elongated leaf shape projection of the crystals synthesized using dC6 and tC6 corresponds to a view down the direction of the straight channels, [010]. The rectangular projection viewed down the thinner dimension of the crystals (Figure 3c and e) corresponds to the [100] direction, along the sinusoidal channels.

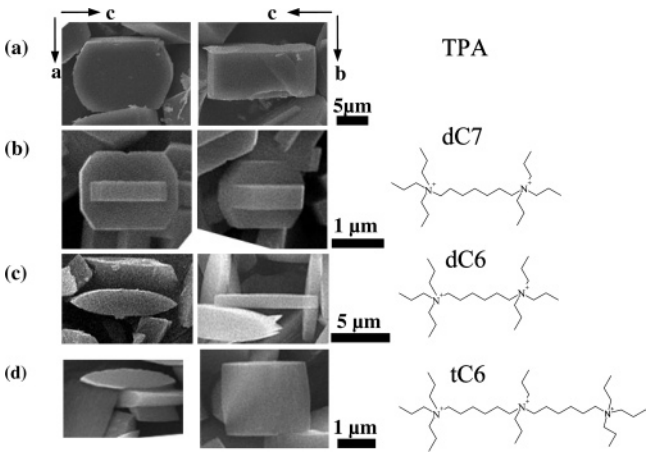

Figure 2. SEM images of silicalite-1: (a) pill- or coffin-shaped crystals using TPA; (b) octagonal shaped crystals with twin intergrowths using dC7; (c) leaf-shaped crystals from dC6; (d) b-elongated leaf-shaped (or platelike) crystals from tC6. The crystallographic directions indicated at the top of the figure are determined by TEM/SAED analysis (see Figure 3).

Crystals synthesized in the presence of dC7 exhibit a well-developed morphology with an octagonal shape (Figure 3a, 2b) that is similar to the shape of TPA grown crystals (Figure 2a) synthesized at similar conditions. While these dC7-grown crystals exhibit twin intergrowths, the crystal dimensions remain in the same order as for the pill- or coffin-shaped TPA-crystals, that is, $L_c \geq L_a > L_b$. Changing the SDA from dC7 to dC6 (with the removal of one CH_2 in the alkyl chain between the nitrogen atoms) yields crystals with $L_c > L_a \approx L_b$ (Figure 3b and c). This relative enhancement for growth along b is even more pronounced with the addition of another TPA unit to the SDA, as tC6 yields b-elongated leaf shaped crystals that approach a platelike morphology with $L_c > L_b > L_a$ (Figure 3d and e). To our knowledge, growth of silicalite-1 using dC7 has not been reported before. Growth of MFI in the presence of dC6

(18) Larson, A. C.; Von Dreele, R. B. *General Structure Analysis System (GSAS)*; Los Alamos National Laboratory: Los Alamos, NM, 2000; pp 86−748.
(19) Toby, B. H. *J. Appl. Crystallogr.* **2001**, *34*, 210−213.

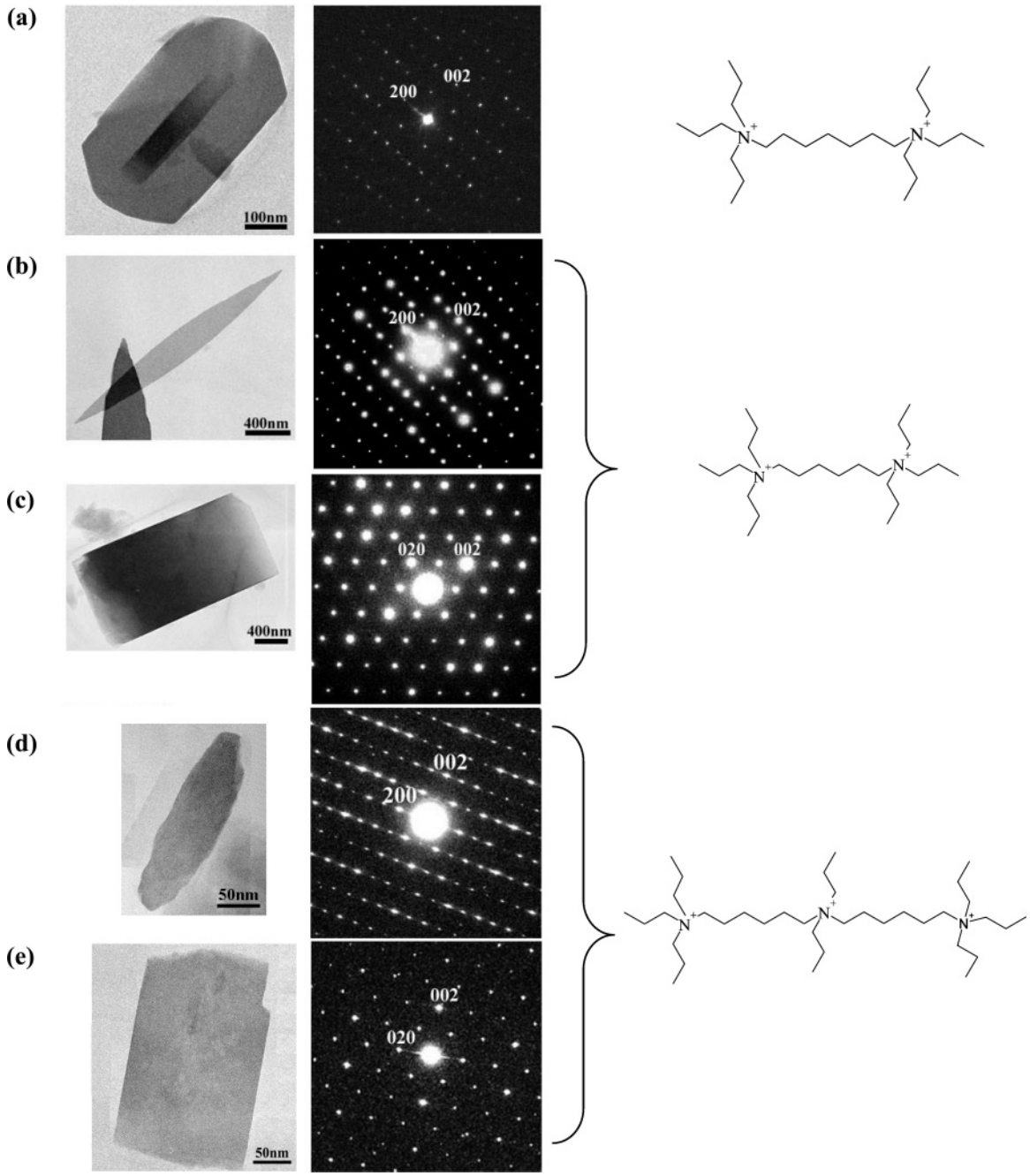

Figure 3. Representative low magnification TEM images and corresponding SAED patterns of calcined zeolite crystals for a synthesis using (a) dC7; (b)−(c) dC6; (d)−(e) tC6. a, b, and d are projections along the [010] direction; c and e are projections along the [100] direction.

has been reported in several studies,[16,17,20−22] and specifically, the same morphology reported here using dC6 is in agreement with the shape reported in ref 17. The use of tC6 for MFI synthesis was introduced by Davis and co-workers.[21,22] Preliminary results on the corresponding morphology[5] are also in agreement with the current findings.

Average values of the crystal aspect ratios for the seeded and nonseeded syntheses were calculated from the corresponding crystal size measurements along the specified crystallographic axes for individual crystals (see Table 2). Although the qualitative trends are the same, the aspect ratios of the crystals from the seeded and nonseeded crystals are different. The difference may be partly due to the size contribution of the colloidal seed (approximately 0.11 μm) to the final size of the product crystals, which biases the final crystal aspect ratio. However, other reasons associated with nucleation and growth kinetics may also play a role in creating these differences. We also present (see Table 2, seeded (corrected)) aspect ratios corrected for the seed particle bias by subtracting the size of the colloidal seed. From the aspect ratios presented in Table 2, we can conclude that although quantitative differences between seeded growth and nonseeded growth exist, the qualitative

(20) Kuhl, G. H.; Hill, C. U.S. Patent 4,585,638, 1986.
(21) Beck, L. W.; Davis, M. E. *Microporous Mesoporous Mater.* **1998**, *22*(1−3), 107−114.
(22) de Moor, P.; Beelen, T. P. M.; van Santen, R. A.; Beck, L. W.; Davis, M. E. *J. Phys. Chem. B* **2000**, *104*(32), 7600−7611.

Table 2. Silicalite-1 Crystal Aspect Ratios for Seeded and Nonseeded Syntheses for Synthesis Conditions Described in Table 1[a]

		L_c/L_a	L_c/L_b	L_a/L_b	$\Delta Ea/b$[d] (kJ/mol)
TPA	seeded	1.1 ± 0.1	2.0 ± 0.1	1.9 ± 0.1	
	seeded (corrected)	1.2 ± 0.1	3.5 ± 0.6	3.5 ± 0.6	
	nonseeded	1.4 ± 0.0	2.4 ± 0.1	1.9 ± 0.1	
dC7	seeded	1.0 ± 0.0	3.4 ± 0.2	3.4 ± 0.2	78.7
	seeded (corrected)	1.1 ± 0.0	[b]	[b]	
	nonseeded	1.3 ± 0.0	3.7 ± 0.1	3.0 ± 0.1	
dC6	seeded				92.5
	seeded (corrected)				
	nonseeded	3.9 ± 0.1	3.5 ± 0.1	0.9[c]	
tC6	seeded	2.2 ± 0.1	1.3 ± 0.1	0.6[c]	
	seeded (corrected)	4.2 ± 0.6	1.4 ± 0.1	0.3[c]	
	nonseeded	4.8 ± 0.1	1.3 ± 0.0	0.3[c]	
dC5	seeded (cylinders)	1.1 ± 0.0	0.7 ± 0.0	0.6 ± 0.0	216.7
	nonseeded (plates)	~0.4	~4	~10	

[a] Corrected aspect ratios for seeded syntheses are calculated by subtracting the dimension of the seed crystals (0.11 μm). Only crystal dimensions greater than 0.14 μm were considered for the corrected aspect ratios (i.e., only crystal dimensions that grew more than 0.03 μm from the original seed crystal were considered). [b] Since growth along the *b*-axis is less than 0.03 μm (within the error of the particle size), reliable calculations cannot be made. [c] L_a/L_b aspect ratios are calculated from the L_c/L_b and L_a/L_b aspect ratios. [d] Difference in energy for SDA located in the sinusoidal versus the straight channel of the zeolite.[17]

trends of crystal aspect ratios are not affected by the presence or absence of seeds for dC7, dC6, and tC6-grown crystals.

Synthesis with dC5. Unlike silicate-1 crystals grown by dC7, dC6, and tC6, crystals synthesized in the presence of dC5 exhibit complex behavior regarding their morphology, crystal size distribution, and so forth. In addition, there are notable differences in the observed crystal morphology for seeded versus nonseeded growth.

Seeded synthesis at 175 °C yields two distinguishable crystal morphologies (Figure 4a) even though XRD analysis confirms that only structure type MFI is present (Suppl. Info. S4). The two morphologies are flat plates and nearly cylindrical crystals. Figure 5 shows a TEM/SAED analysis of the cylindrical crystals. The flat nearly circular projection shown in the low magnification TEM image (upper left part of Figure 5) corresponds to an electron diffraction pattern indexed as [010] zone axis. This means that the *b*-axis (straight channels) is along the largest dimension of the crystal. This is corroborated by the TEM and SAED along the [100] zone axis shown in the lower part of Figure 5. From this analysis, it is clear that for these silicalite-1 crystals $L_b > L_c \geq L_a$. To our knowledge, this is the first observation of a silicalite-1 morphology with the largest crystal dimension along the *b*-axis (L_b). Crystal sizes and aspect ratios of these newly observed cylindrical crystals are listed in Tables 1 and 2, respectively. In contrast to the cylindrical crystals, a TEM/SAED analysis reveals that the flat plates synthesized at 175 °C have their shortest dimension along the *b*-axis (Suppl. Info. S5). Because of their irregular shape, it was not possible to determine the crystal dimensions along the *a*- and *c*-axes.

Nonseeded crystallization at 175 °C yields only well-developed flat plate crystals (Figure 4b), resembling those obtained in seeded synthesis (Figure 4a). Figure 6 shows the TEM/SAED analysis of these flat plate crystals viewed along the [010] zone axis (i.e., the *b* direction). Here, identification of the crystal size along the *a*- and *c*-axes was possible. Interestingly, the crystal size along the *a*-axis (L_a) is now the largest ($L_a > L_c > L_b$). To our knowledge, this is also the first time that such a sequence of crystal dimensions is reported for silicalite-1. The sizes of these flat plate crystals synthesized in the presence of dC5 range from 10 to 20 μm along the *a*-axis, 3−8 μm along the *c*-axis, and 1.0−2.0 μm along the *b*-axis (a statistical analysis was not

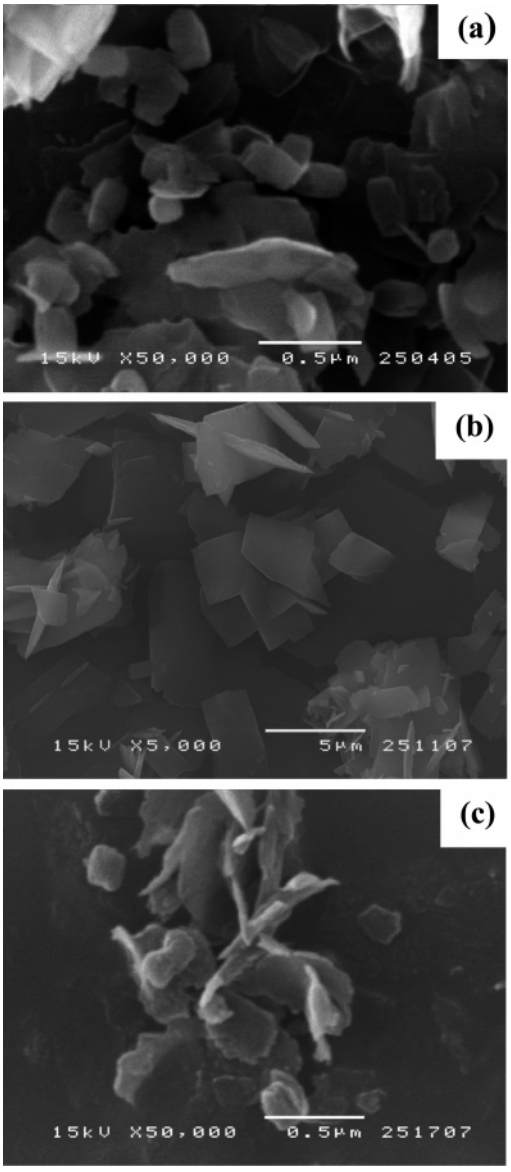

Figure 4. Representative SEM images of as-made samples synthesized in the presence of dC5: (a) seeded at 175 °C; (b) nonseeded at 175 °C; (c) seeded at 130 °C.

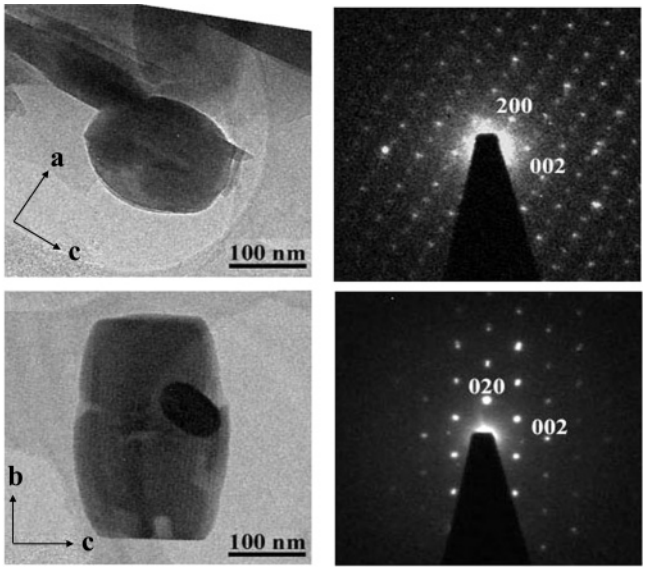

Figure 5. Low magnification TEM images and corresponding SAED patterns along the direction parallel to the straight channels, [010] (top), and sinusoidal channels, [100] (bottom), of typical calcined cylindrical shaped crystals from a seeded synthesis at 175 °C using dC5.

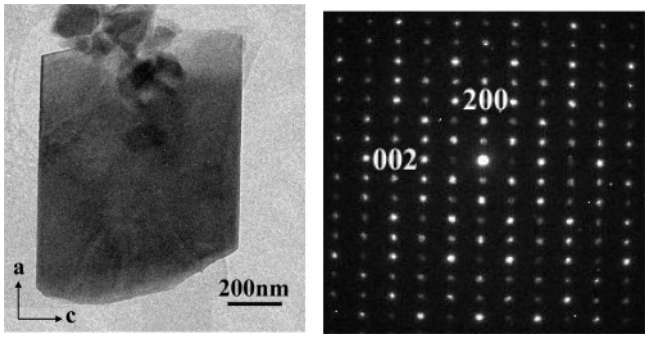

Figure 6. TEM/SAED analysis of a typical calcined flat plate shaped crystal from a nonseeded synthesis at 175 °C using dC5. The commonly observed [010] pattern confirms the shortest dimension is along the *b*-axis such that the new order of crystal dimensions is $L_a > L_c > L_b$.

performed for these crystals). An XRD analysis indicates that only structure type MFI is present (Supp. Info. S4).

From the $^{13}C-CP$ MAS NMR spectra, it is possible to observe decomposition of dC5 when the zeolite synthesis temperature is 175 °C for both seeded and nonseeded synthesis. While the solid-state spectrum shown in Figure 7c has about 10 peaks, the liquid spectrum has only 6 (Figure 7a). An analysis of the spectra indicates that these peaks may be due to decomposition by Hofmann degradation of the dC5 that will give an olefin, water, and tertiary amine. The presence of the olefin is supported by peaks at 117.5 and 136.9 ppm for seeded synthesis. While further experiments are required to fully characterize the organic material occluded in the zeolite, these spectra clearly show that the dC5 cation has limited stability at these synthesis conditions. Therefore, to avoid dC5 decomposition, seeded and nonseeded syntheses of silicalite-1 in the presence of dC5 were also performed at the lower temperature of 130 °C. For both seeded and nonseeded synthesis at 130 °C, the solid-state ^{13}C NMR spectra shows the same number of peaks as the aqueous iodide salt, although the peaks are shifted and broadened. From these spectra, we can conclude that the dC5 does not decompose during synthesis at 130 °C and is located intact inside the silicalite-1 framework of the crystals synthesized at this lower temperature.

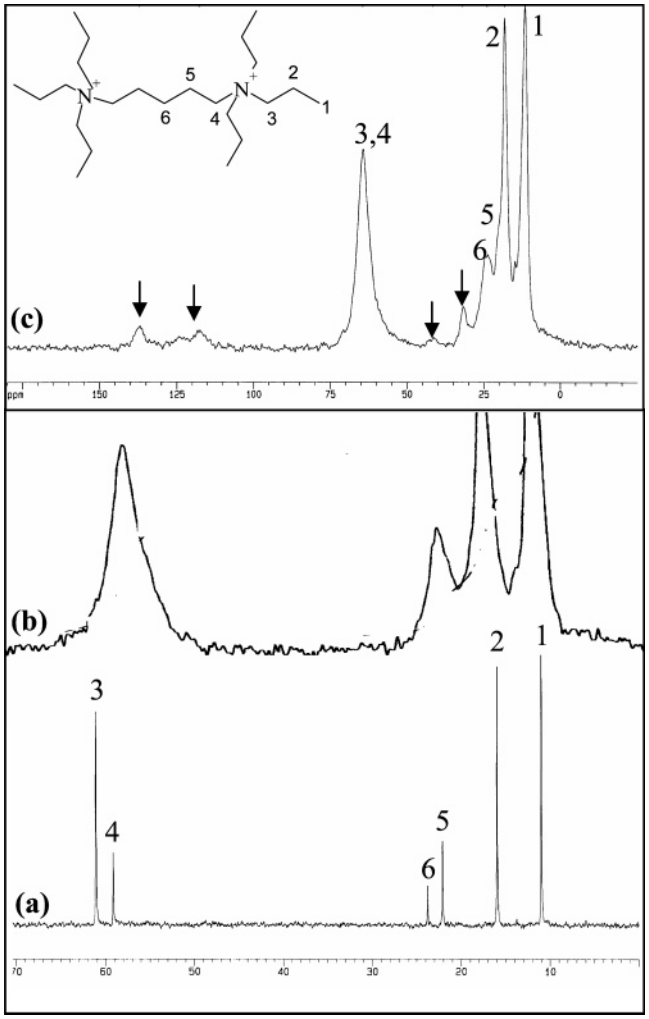

Figure 7. (a) ^{13}C NMR liquid spectrum of an aqueous solution of dC5 iodide. Solid-state ^{13}C NMR spectrum of uncalcined zeolite crystals from a seeded synthesis in the presence of the dC5 iodide with a molar composition of $40SiO_2$:7.5dC5:24.5KOH:$9500H_2O$:160EtOH at (b) 130 °C for 48 h and (c) at 175 °C for 3.6 days (images have different scales). Peaks marked with the arrows do not belong to the original template in solution and indicate limited stability of the dC5 cation at 175 °C.

Seeded synthesis at 130 °C yields crystals in the form of cylinders as well as plates (sheetlike) (Figure 4c). An XRD analysis shows that the only crystalline material present is MFI (Supp. Info. S1d). A TEM/SAED analysis of the cylindrical crystals synthesized at 130 °C along the [010] and [100] zone axes of the crystal (i.e., the *a*- and *b*-directions, respectively) demonstrates that the morphology is similar to that of the cylinders synthesized at 175 °C (Supp. Info. S6).

Figure 8 shows a TEM/SAED analysis of the sheetlike morphology. Figure 8a shows a typical extended sheet supporting several smaller cylindrical crystals. The higher magnification TEM image shown in Figure 8b along with its corresponding SAED pattern (Figure 8c) indicates that the sheets are crystalline with a *d* spacing of ~10 Å as the largest spacing in this projection. This *d* spacing, consistent with the MFI structure, along with the absence of reflections other than those of MFI in

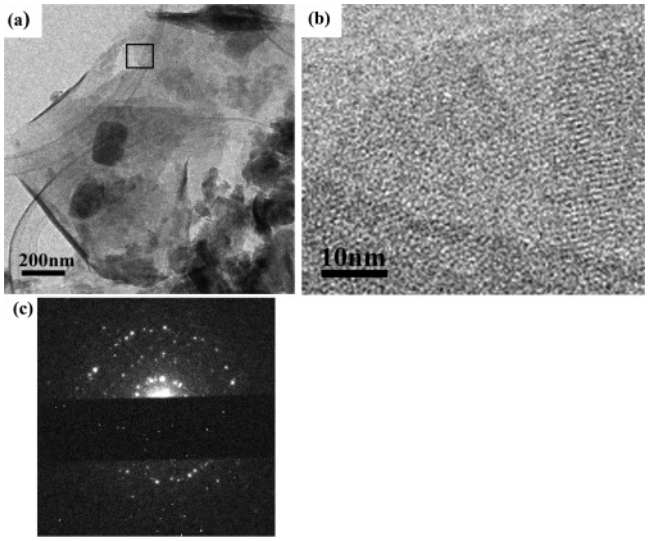

Figure 8. TEM/SAED analysis of typical sheetlike morphology from a nonseeded synthesis at 130 °C using dC5: (a) low magnification image of the sheetlike and cylindrical shaped crystals; (b) high magnification image of the sheetlike morphology (from the area marked by the rectangle in a) showing fringes indicative of crystalline order; (c) SAED from sheet morphology indicating *d* spacing consistent with the MFI structure type.

the XRD pattern, suggests that the sheets are MFI crystals as well. Therefore, it appears that the synthesis of MFI in the presence of dC5 leads to a competition of two morphologies, that is, cylinders and flat plates or sheets, with a pronounced difference in the crystal aspect ratios. The qualitative similarity of crystal morphologies obtained at 130 °C (no dC5 decomposition) and 175 °C (some dC5 decomposition) makes the possibility of two morphologies due to dC5 decomposition a less likely scenario. Instead, we believe that the two morphologies are a result of competition between growth of the added seeds (leading to cylinders) and growth of new nuclei (leading to plates). This assignment is further supported by the absence of cylinders in nonseeded growth. Moreover, in several of the TEM images of cylindrical MFI crystals (see, for example, the darker part in the crystal shown in Figure 5, bottom left), we observed contrast that can be attributed to slightly different orientations of crystal portions corresponding to a seed core and outer shell grown on the seed.

Summary of Obtained Morphologies and Importance for Potential Applications. Two new morphologies that are drastically different from the typical TPA-silicalite-1 morphology ($L_c \geq L_a > L_b$) were synthesized in pure form using tC6 (platelike leaf-shaped crystals with $L_c > L_b > L_a$) and dC5 (platelike crystals with $L_a > L_c > L_b$). A third morphology with $L_b > L_c \geq L_a$, the first reported with the straight channels of MFI running along the longest crystal dimension, was identified. However, it was only obtained along with sheetlike crystals in seeded growth using dC5. As argued above, we believe that the cylindrical morphology is a result of direct growth of MFI seeds.

Our interest in these morphologies stems mainly from their potential use in preparing permselective molecular sieve coatings. In refs 5 and 23−25, we have shown that control of the preferred orientation and microstructure (grain size, film thickness, etc.) of zeolite films can have considerable effects on the membrane performance, that is, permeation rate, selectivity, and stability. We have already used tC6 to grow *b*-oriented monolayers of silicalite-1 crystals to form *b*-oriented MFI films.[5] The *b*-oriented seed layer in this case was developed exploiting the shape (shortest dimension along the *b*-axis) of TPA-MFI seeds. We believe that the new morphologies described here may enable improved performance MFI films. Although considerable experimentation will be needed to explore this potential, at this stage we can argue that (1) seeding with the thin platelike crystals made by dC5 provides a route to thinner films with larger grain size (reduced number of grain boundaries), (2) seeding with tC6-grown crystals opens the possibility of *a*-oriented seed layers and eventually *a*-oriented MFI films, and (3) the cylindrical morphology obtained when using dC5 in the presence of MFI seeds may allow growth of *b*-oriented MFI films from randomly oriented seed layers by van der Drifts growth.[5]

In addition to offering new directions for microstructural control of zeolite films, the morphologies described here can contribute to the understanding of zeolite growth as discussed below.

Interpretation of Morphology Based on SDA/Framework Interactions. The experimental results reported here are a long overdue follow up of the pioneering modeling study by de Vos Burchart et al.[17] In this study, the relative crystal size along the *a*- and *b*-axes has been interpreted in terms of how well the SDA fits in the straight (*b*-axis) versus the sinusoidal (*a*-axis) channels.[17] Molecular mechanics simulations suggested that for all dimers, the straight channels are the favored location with an increased preference for the straight channels in the order dC7 < dC6 < dC5.[17] This is indicated by the corresponding $\Delta Ea/b$ (from ref 17) shown in the last column of Table 1. $\Delta Ea/b$ is the calculated energy difference of the most favored configuration with the dimer extending in the sinusoidal minus that of the dimer along the straight channel. The large differences indicate that the dimers will be located with their long dimension almost exclusively extending along the *b*-axis. To attain such a configuration, the SDA should adsorb with one propyl chain inside a straight channel. If the preferential location of the SDA inside the straight channels of the zeolite was solely responsible for the crystal morphology, then an increase in the crystal size along the *b*-axis, relative to TPA, should be observed for all of the dimers. An inspection of the last two columns of Table 1 indicates that this is the case for dC5 (cylinders) and dC6, that is, a better SDA fit in the straight channel is in agreement with the enhancement of growth along *b* relative to growth along *a* (L_a/L_b for TPA > L_a/L_b for dC6 > L_a/L_b for dC5 (cylinders)). While simulations are not available for the tC6, we expect that its preference for the straight channel versus the sinusoidal channel would be more pronounced than that of dC6 in agreement with the experimental findings (L_a/L_b for dC6 > L_a/L_b for tC6). Therefore, the observed L_a/L_b ratios for dC6, tC6, and

(23) Gouzinis, A.; Tsapatsis, M. *Chem. Mater.* **1998**, *10*(9), 2497−2504.
(24) Lovallo, M. C.; Tsapatsis, M. *AIChe J.* **1996**, *42*(11), 3020−3029.
(25) Xomeritakis, G.; Lai, Z. P.; Tsapatsis, M. *Ind. Eng. Chem. Res.* **2001**, *40*(2), 544−552.

dC5 (cylinders) are in agreement with the expected behavior on the basis of the preference of the SDA to extend along the straight versus sinusoidal channels. However, this is not the case for dC7 since the relative growth along the *b*-axis is the slowest and L_a/L_b is even larger than that for TPA. Also, in sharp disagreement with the expected behavior is the plate- (and sheet-) like morphology obtained in the presence of dC5.

While the combination of experimental and modeling[17] studies provide valuable insights into the ratio of the growth rates along the *a*- and *b*-axes, this is not the case for understanding the growth behavior along the *c*-axis. Up to now, it was thought the fastest growth direction[17] is always along the *c*-axis in agreement with simple crystal growth arguments, like the Bravais−Friedel−Donnay−Harker law, that suggest the growth rate along a crystallographic direction is inversely proportional to the corresponding *d* spacing. To our knowledge, the MFI morphologies observed using dC5 are the first ones with L_c considerably smaller than another crystal dimension. Therefore, further theoretical and modeling studies are needed to understand this behavior.

The SDAs also have an impact on nucleation kinetics. In a set of nonseeded experiments at 175 °C, the induction times for dC6, dC7, and tC6 were approximately 0.7, 0.5, and 6.4 h, respectively. Moreover, dC5 did not yield zeolite crystals with the intact cation under nonseeded conditions at 175 °C. These results are in agreement with the previously reported predictions[17] that suggest that dC7 fits better in the zeolite pores compared to dC6, while dC5 is not readily accommodated.

To address further this last point, we report preliminary estimation of lattice constants from refinement of the synchrotron X-ray data. In Figure 9, we report the experimentally determined lattice constants (refined from the data of Supp. Info. S2) for all the SDAs and compare the unit cell volumes with those predicted by the modeling in ref 17, for SDAs located in the straight channels. The experimental results show that the different crystal morphologies have different lattice parameters with the variation along the *c*-axis being most pronounced (~1% vs 0.3 and 0.5% for the *a*- and *b*-axes). As a result, the unit cell volume varies by about 1% depending on the crystal morphology obtained. The experimentally derived variations are significantly more pronounced when compared with the predictions of ref 17 indicating that calculation of host−guest interaction should be revisited.

To summarize, comparison with previously reported predictions[16,17] indicates that while the fit of the SDA in the zeolite channels is a major factor affecting the crystal shape, it can only partly account for the experimental findings. More specifically, although crystal shape modification by use of dC6 and tC6 can be captured, the use of dC7 and dC5 gives rise to unexpected behavior. This suggests that in addition to the fitting of the SDA in the MFI structure, processes such as adsorption/desorption of the SDA and the effects of silica speciation and precursor subcolloidal particles may also be important. Moreover, the variation of unit cell dimensions from XRD data is more pronounced compared to model predictions and point to a need for reexaminination of the host−guest interaction between MFI framework and the SDAs.

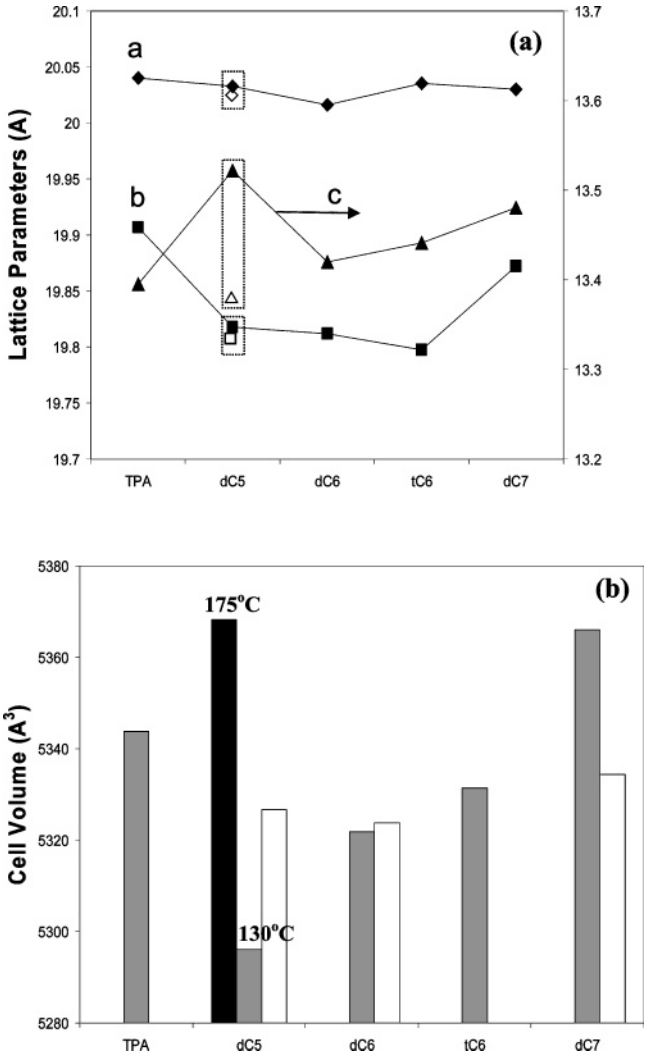

Figure 9. (a) Lattice parameters refined from synchrotron XRD (filled symbols are from synthesis at 175 °C and open symbols are from synthesis at 130 °C using dC5). (b) Unit cell volumes in comparison with the predicted values of ref 17 (darker shade columns: experimental refined values, lighter shade columns: predicted values). For dC5 the black (first) column corresponds to synthesis at 175 °C and the middle column to synthesis at 130 °C.

Conclusions

New crystal morphologies of an important zeolite catalyst, adsorbent, and molecular sieve membrane material (siliceous ZSM-5) are reported indicating that growth rates along the three main crystal directions can be controlled by SDA design. In contrast to the well-known silicalite-1 crystal morphology with the longest crystal dimension along the *c*-axis, crystals with the longest dimension along the *a*- and *b*-axis were obtained by using oligomeric SDAs. These new morphologies lead to new directions for microstructural control of molecular sieve films.

While a comparison with previous modeling studies indicates that the fit of the SDA in the zeolite framework provides guidelines for crystal shape modification,

it cannot account for all of the observed morphologies pointing to the need for additional modeling work.

Acknowledgment. The authors acknowledge J. Pérez-Pariente and O. Terasaki for providing access to TEM facilities. I.D. acknowledges the MECD/Fulbright Postdoctoral Fellowship. Funding for this work was provided by NSF/NIRT (CTS-0103010) and NASA-Microgravity (98 HEDS-05-218). Research carried out in part at the NSLS at BNL is supported by the U.S. DOE (DE-Ac02-98CH10886 for beamline X7A).

Supporting Information Available: XRD patterns and refinement, ^{13}C NMR spectra, and some SEM/TEM/SAED analysis (pdf). This material is available free of charge via the Internet at http://pubs.acs.org.

CM048854W